Lawrence Berkeley National Laboratory

Molecular Biophys & Integ Bi

Title

Sponge-Like Li4Ti5O12 Constructed on Graphene for High Li Electroactivities

Permalink

Journal

ISSN

Authors

Bae, Seongjun
Nam, Inho
Park, Soomin
et al.

Publication Date

DOI

Sponge-Like Li$_4$Ti$_5$O$_{12}$ Constructed on Graphene for High Li Electroactivities

Seongjun Bae[1,2], Inho Nam[1,2], Soomin Park[1,2], Young Geun Yoo[1,2], Jongseok Park[1,2], Jong Min Lee[2], Jeong Woo Han[3], and Jongheop Yi[1,2,*]

[1] *World Class University (WCU) Program of Chemical Convergence for Energy and Environment (C2E2), Institute of Chemical Processes, Seoul National University, Seoul 151-742, Republic of Korea*
[2] *School of Chemical and Biological Engineering, Seoul National University, Seoul 151-742, Republic of Korea*
[3] *Department of Chemical Engineering, University of Seoul, Seoul 130-743, Republic of Korea*

A sponge-like Li$_4$Ti$_5$O$_{12}$/graphene composite was prepared via sequential hydrothermal process and solid-state heat treatment process for the application to high-power lithium ion batteries. The as-prepared electrode showed outstanding Li electroactivities with a rapid and reversible Li insertion/ extraction of up to 10 C-rate (1.75 A/g). It delivered a discharge capacity of 174 mAh/g at 0.5 C, near the theoretical capacity of Li$_4$Ti$_5$O$_{12}$, with good rate capability and cyclic stability. First-principles calculations revealed the intimate interaction of the Li$_4$Ti$_5$O$_{12}$ and graphene, which implies that graphene functions as an 'electron tunnel.' Electrochemical impedance spectroscopy also proved that the graphene-hybridization and the unique structure of the Li$_4$Ti$_5$O$_{12}$ material significantly reduce the resistive behavior of electrodes. The 3D structured Li$_4$Ti$_5$O$_{12}$/graphene hybrid reported herein could be a promising candidate for a safe, low-cost, high-power anode for lithium ion batteries, and our seeding-growth-sintering method for decorating graphene with active material will offer an effective upgrade on highly insulating Li$_4$Ti$_5$O$_{12}$ materials.

Keywords: Lithium Ion Battery, Anode, Li$_4$Ti$_5$O$_{12}$, Graphene, Nanostructure.

1. INTRODUCTION

Lithium ion batteries (LIBs) are a general power source that are used in mobile electronic devices due to their high energy and power density. The increasing demand for heavy-duty electronic vehicles has stimulated the development of advanced LIBs that are safe to use and show a high rate performance.[1–3] Although graphite, the most commercially used anode for LIBs, has a high conductivity and a reliable theoretical capacity (373 mAh/g), it cannot satisfy the requirements for high-power applications because its surface is very reactive during charging or discharging at a low operating voltage (0.2 V vs. Li/Li$^+$). This phenomena result by the formation of an unstable solid surface interface (SEI) that is produced from a reaction between the graphite and the electrolyte.[4–6] Therefore, safety issues associated with the use of graphite anodes cannot be ignored during high rate operations.

The safety risk originated from the decomposition of electrolyte can be circumvented by adopting a titanate compound as an anode material which has a high operating voltage (>1.0 V vs. Li/Li$^+$). The high operating voltage of titanate-based anode materials also ensures proper application of them to bipolar battery system, to the exclusion of the formation of Li/Al alloy (0.4 V vs. Li/Li$^+$).[7] In addition, titanate compounds are chemically/physically stable, inexpensive and non-toxic.[8–11] The most well-known titanate compound is lithium titanium oxide (Li$_4$Ti$_5$O$_{12}$, LTO). LTO has a stable working potential (~1.55 V vs. Li/Li$^+$) and outstanding reversibility and cyclability. Nevertheless, its intrinsically poor conductivity is generally regarded as a major obstacle to widespread applications.[12,13]

In this regard, many attempts have been made to improve electron and ion conductivities of LTO. Nanostructuring is an effective strategy for achieving this, because the decrease in the overall diffusion path inside crystals can dramatically accelerate the migration of charge carriers.[14–16] The use of carbon additives, especially, hybridization with graphene, also has been considered as an alternative strategy, since their use results in a significant

improvement in rate performance due to the enhanced electronic conductivity.[17–20] However, the combined usage of the two strategies continues to be a challenge, which can be attributed to the difference in dimension between the active materials (0D, 3D) and graphene (2D). Therefore, the development of an ingenious design and synthetic process is required to produce nanostructured LTO/graphene composites for high-power applications.

Herein, we report on the synthesis of sponge-like LTO/graphene (s-LTO/graphene) composites from the TiO$_2$ nanorods/graphene composite by inducing the asymmetric growth of TiO$_2$ during a hydrothermal reaction. Then the TiO$_2$ in composite is converted to LTO by means of a solid-state heating method. The s-LTO/graphene composite showed enhanced Li electroactivities. Detailed synthetic procedures and mechanistic studies of the improved electrochemical properties are discussed below.

2. EXPERIMENTAL DETAILS

To fabricate primary TiO$_2$ particles/graphene oxide (GO), 100 ml of an aqueous solution containing 50 mg GO, prepared by an improved Hummer's method[21] was sonicated for 1 h. A mixture of 1 ml titanium isopropoxide (TTIP) and 10 ml ethylene glycol was then slowly added to the GO solution. The mixture was washed with water and isolated by centrifugation (2500 rpm, 5 min), and dried at 60 °C for 12 h. A 50 mg sample of dried TiO$_2$/GO was mixed with 20 ml of a 26 M HCl solution and 0.2 ml of TTIP was added. The suspension was transferred to a 100 ml autoclave and allowed to react at 150 °C for 18 h to induce asymmetric growth of TiO$_2$ nanorods/graphene. After the hydrothermal reaction, the sample was washed with water and dried. The stoichiometric mixture of TiO$_2$ nanorods/graphene (0.2 g) and lithium carbonate (0.0185 g) was heated at 850 °C for 2 h under a N$_2$/H$_2$ atmosphere to produce the s-LTO/graphene.

The morphology of the samples was examined by transmission electron microscopy (TEM, JEOL, JEM-2100F)

and scanning electron microscopy (SEM, Carl Zeiss, SUPRA 55VP). The crystallinity of the samples was analyzed using an X-ray diffractometer (XRD, Rigaku, D/max-2200). Thermogravimetric analysis (TGA, TA Instruments, Q-500 IR) was utilized to determine the graphene content.

The electrochemical performance of the preparations was analyzed using a coin cell (CR2032). A coin cell was assembled in Ar-filled glove box. Lithium foil, a polypropylene membrane, and 1.15 M LiPF$_6$ solution dissolved in 3:5:2 (v/v/v) ethylene carbonate/ethyl-methyl carbonate/diethyl carbonate were used as the counter electrode, separator and electrolyte, respectively. A working electrode was prepared by mixing 80 wt% of the active material, 10 wt% super P as conducting carbon and 10 wt% poly(vinylidene difluoride) as a binder. The mixture was blended with a few drops of N-methyl-2-pyrrolidone. The slurry was cast on Cu foil using a doctor blade and dried under a vacuum at 120 °C for 12 h. Galvanostatic charge/discharge was performed by an automatic battery cycler (WBCS3000, Wonatech). Electrochemical impedance spectroscopy (EIS) was conducted using a computer-controlled potentiostat (ZIVE SP2, Wonatech) at 1.55 V. EIS was conducted from 10 mHz to 100 kHz with a 10 mV amplitude under AC stimulus. The equivalent circuit was fitted using the ZMAN software to quantify the parameters.

Periodic density functional theory (DFT) was used for first-principles calculations. Generalized gradient approximation (GGA) within the Perdew-Burke_Ernzerhof (PBE) exchange-correction functional was applied to the calculations.[22, 23] Ionic cores were described by the projector-augmented wave (PAW) method using the Vienna *ab-initio* simulation package (VASP).[24] Van der Waals interactions were incorporated using the DFT-D2 empirical correction of Grimme.[25] Coulombic interactions of the localized d orbital of Ti atoms were calculated by
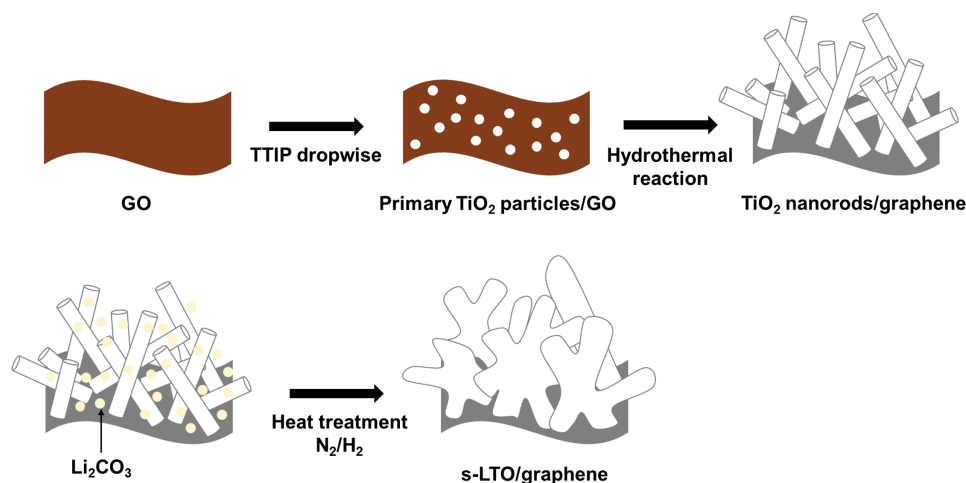
Figure 1. Schematic illustration showing the synthesis of s-LTO/graphene.

DFT $+ U$ ($U_{\text{eff}} = 3.5$) within Dudarev's approach.[26] The energy cutoff was 400 eV and $1 \times 1 \times 1$ k-point mesh was used in Monkhorst-Pack method.

3. RESULTS AND DISCUSSION

Schematic illustration describing the synthesis of s-LTO/graphene is shown in Figure 1. The primary TiO$_2$ particles/GO composite was synthesized by inducing a hydrolysis-condensation reaction of TTIP on the surface of the GO. Because the hydrolysis of the TTIP in water is so fast, the direct mixing of TTIP with the GO solution results in the separation of TiO$_2$ and GO. In order to prevent such a separation and to secure intimate contact between the GO and primary TiO$_2$ particles, ethylene glycol was utilized to reduce the reactivity of TTIP.[27] As a result, TiO$_2$ seeds were formed as functional groups (–COOH, –OH) on the GO.[28] During the hydrothermal reaction, the reduction of GO to reduced graphene oxide (graphene) and the secondary growth of primary TiO$_2$ particles to TiO$_2$ nanorods were achieved. For the conversion to LTO/graphene, the TiO$_2$ nanorods/graphene was heat-treated under a H$_2$/N$_2$ atmosphere. The high temperature induces sintering of the LTO particles, which forms interconnected linkages between TiO$_2$ nanorods, producing an LTO network with a sponge-like structure.

XRD patterns of sample are shown in Figure 2(a). The primary TiO$_2$ particles/GO shows a broad peak corresponding to anatase (JCPDS card 21-1272). Peaks corresponding to rutile (JCPDS card 21-1276) and anatase phase were observed for the TiO$_2$ nanorods/graphene preparation. The diffraction pattern of s-LTO/graphene after the conversion from the TiO$_2$/graphene clearly indicates that it contains a spinel LTO structure (JCPDS card 49-0207). No TiO$_2$ peak was observed for the s-LTO/graphene, which confirms that the TiO$_2$ was completely converted into LTO. The LTO peaks were relatively sharp compared to those of TiO$_2$ nanorods because the heat treatment process causes the sintering of LTO crystallites. The absence of peaks corresponding to graphite reveals that the re-stacking of graphene was prevented by the presence of the anchored active material. According to the result of TGA, weight loss occurred in range of 400~500 °C, which is caused by
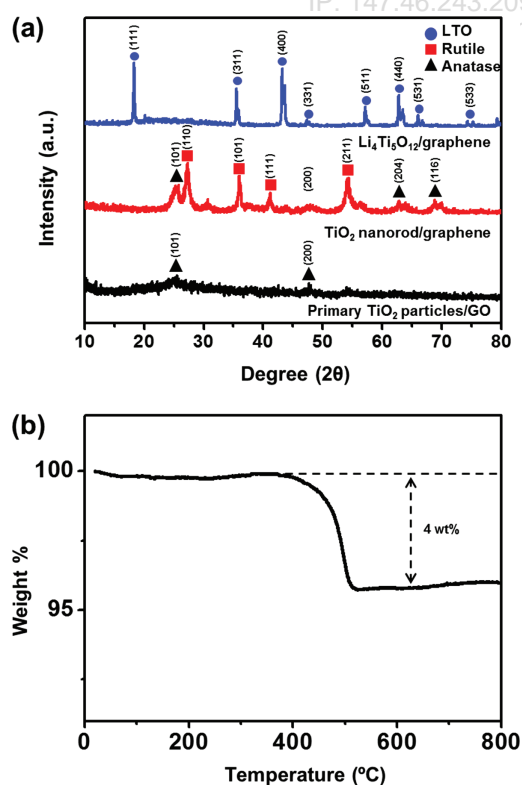

Figure 2. (a) XRD patterns of primary TiO$_2$ particles/graphene, TiO$_2$ nanorods/graphene and s-LTO/graphene, and (b) TGA result for s-LTO/graphene.
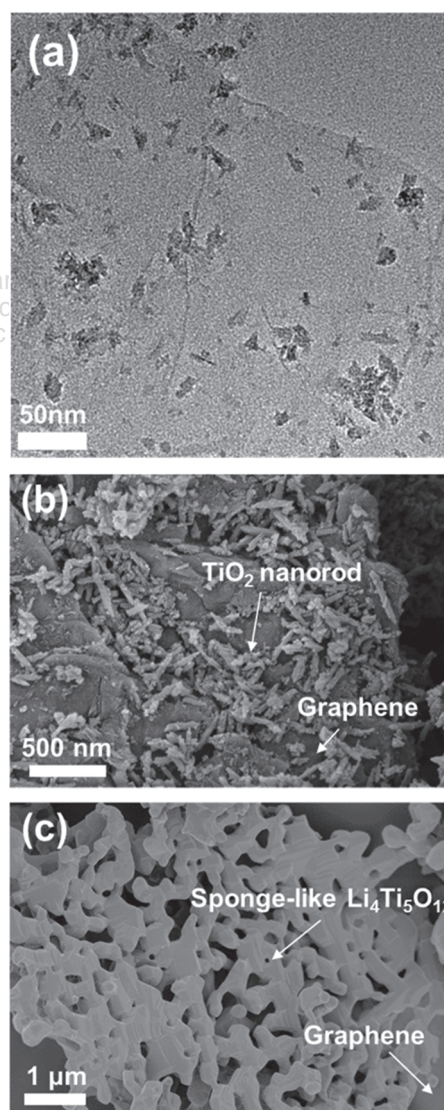

Figure 3. TEM image of (a) primary TiO$_2$ particles/GO, SEM images of (b) TiO$_2$ nanorods/graphene and (c) s-LTO/graphene.
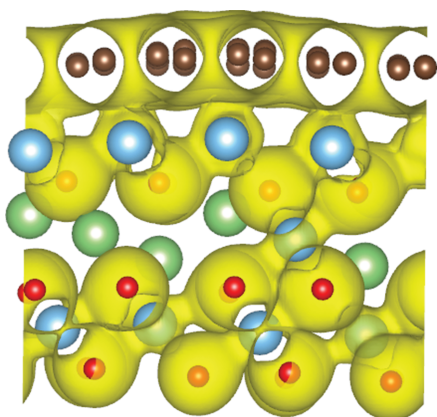
Figure 4. Charge density of the LTO/graphene interface. The isosurface is 3×10^{-2} e/a$_0^3$.

the decomposition of graphene.[29, 30] The graphene content was determined to be 4 wt% in the s-LTO/graphene.

Figure 3 shows the morphological analyses of the synthesized TiO$_2$/graphene and the s-LTO/graphene by TEM and SEM. TEM image (Fig. 3(a)) indicates that TiO$_2$ nanoparticles are well-distributed on the GO. The size of the TiO$_2$ attached to the surface of the GO is about 5 nm. After the hydrothermal reaction of TiO$_2$ under highly acidic conditions (2 M HCl), asymmetrically grown nanorods were observed on the graphene sheet. As shown in Figure 3(b), the width of the nanorod is about 30 nm and length is about 200∼300 nm. The entangled TiO$_2$ nanorods cause the conversion to LTO/graphene with sponge-like structures. During the sintering process for the synthesis of s-LTO/graphene, the TiO$_2$ nanorods become

linked and the three dimensional porous structure of LTO is formed. As seen in Figure 3(c), sponge-like structure is produced.

The localization of electrons at the interface between the graphene and LTO was investigated by first-principles calculations. Figure 4 shows the charge density of constructed model that contains the (111) plane of LTO in company with the graphene. It is obvious that electronic hybridization is generated between the orbital of carbon atoms constituting the graphene and Ti atoms on the outermost layers of LTO. This result indicates the existence of a strong interaction between the graphene and Ti-based materials, suggesting that the graphene can be used as an 'electron tunnel.' Therefore, the synthesized composite shows a higher conductivity than pure materials without graphene. The calculated binding energy is 85 meV/Å^2.

The electrochemical properties of s-LTO/graphene and sponge-like LTO without graphene (pure LTO) as anode materials for LIB were evaluated and the results are shown in Figures 5–7. Galvanostastic charge/discharge tests were performed at 0.5, 1, 5 and 10 C in a potential window of 1∼3 V. The charge/discharge voltage profiles of both s-LTO/graphene and pure LTO show a flat plateau near 1.55 V which attributed to the phase transition from spinel to rock-salt (Fig. 5). The smaller level of polarization demonstrates that s-LTO/graphene maintained superior conductivity and reversibility even at high-rate charge/discharge process. The s-LTO/graphene shows discharge capacities of 174.2, 172.6, 134.2 and 110.7 mAh/g at 0.5, 1, 5 and 10 C, respectively (Fig. 6(a)). The value of 174.2 mAh/g at 0.5 C is almost the same as the value for the theoretical capacity of pure LTO (175 mAh/g).
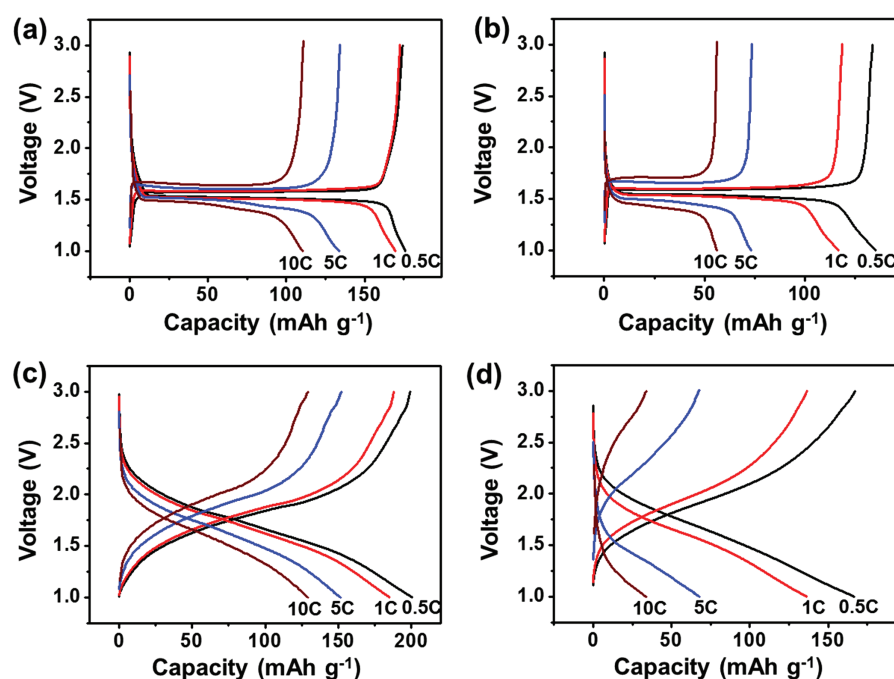
Figure 5. Charge/discharge curves for (a) s-LTO/graphene, (b) pure LTO, (c) TiO$_2$ nanorods/graphene and (d) TiO$_2$ nanorods.
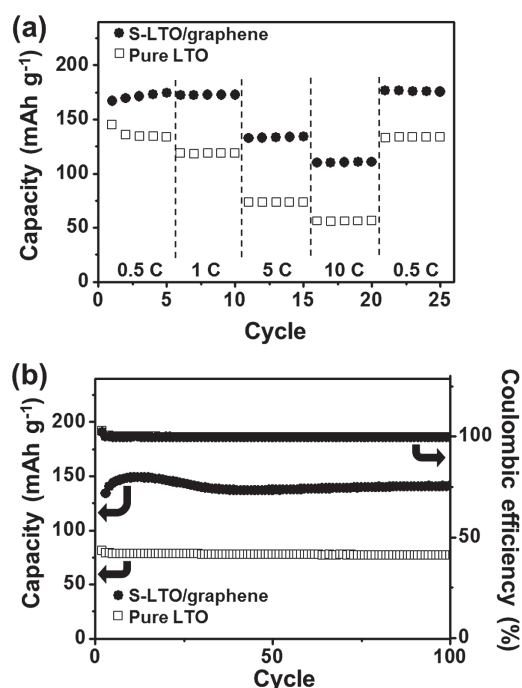
Figure 6. (a) Rate capability of s-LTO/graphene and pure LTO and (b) long cycle performance test and Coulombic efficiency analysis of s-LTO/graphene and pure LTO.

The capacity of the s-LTO/graphene is found to be superior to that of the pure LTO synthesized using TiO$_2$ nanorods (133.7, 118.7, 73.5 and 56.3 mAh/g) because graphene enhances the electrical conductivity of the overall electrode. Figure 6(b) shows the long cycle performances of LTO electrodes at 5 C. The results clearly show that s-LTO/graphene have a stable capacity at a high rate. The Coulombic efficiency reached more than 99%, indicating that the intercalation/de-intercalation reaction in s-LTO/graphene is highly reversible. Although TiO$_2$ shows
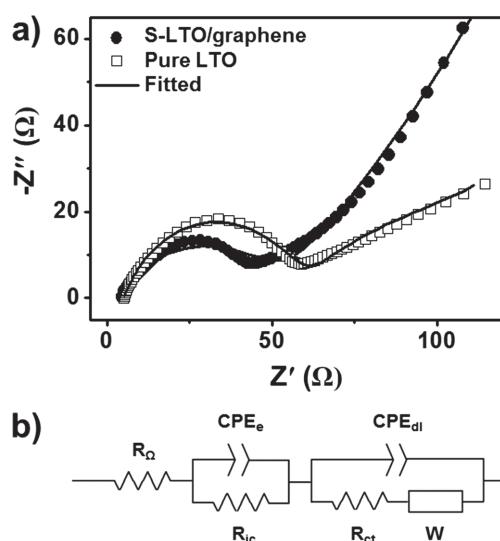

Figure 7. (a) Nyquist plots of s-LTO/graphene and pure LTO and (b) Equivalent circuit.

Table I. Resistance values of equivalent circuit.

	$R_\Omega(\Omega)$	$R_{ic}(\Omega)$	$R_{ct}(\Omega)$
s-LTO/graphene	2.7	51.3	42.3
Pure LTO	5	74.5	53.4

a typical voltage sloping charge/discharge profile from 1 V to 2 V, TiO$_2$ nanorods/graphene can also be used as anode materials for lithium ion batteries. As seen by Figures 5(c and d) the reversible capacity of the TiO$_2$ nanorods/graphene was determined to be 199.2, 188.1, 151.9 and 129.1 mAh/g at 0.5, 1, 5 and 10 C, respectively. In contrast, the capacity of the TiO$_2$ nanorods rapidly decreased from 167.2 mAh/g to 34.1 mAh/g at 0.5 and 10 C.

The increase in conductivity induced by graphene can be verified by EIS. Figure 7 shows Nyquist plots and fitted equivalent circuit model. R_Ω, R_{ic} and R_{ct} are the kinetic parameters corresponding to the resistance of the cell, intercrystal resistance and charge transfer resistance of the electrolyte/electrode, respectively. CPE$_e$ and CPE$_{dl}$ are the non-ideal capacitive element of the surface of the active materials and an electric double layer capacitor. W is the Warburg impedance. The quantified resistances are summarized in Table I. The R_{ct} value for the s-LTO/graphene is smaller than those of pure LTO, which verifies the positive contribution of graphene to the excellent conductivity of the product.

4. CONCLUSION

TiO$_2$ nanorods/graphene was prepared by a hydrothermal method and TiO$_2$ attached on the graphene was directly converted to LTO. The LTO had a sponge-like structure due to the interconnected linkages of the TiO$_2$ nanorods. The s-LTO/graphene composite showed a high capacity, rate capability and excellent conductivity compared to pure LTO, which can be attributed to the presence of an electron-gathering graphene sheet.

References and Notes

1. K. Kang, Y. S. Meng, J. Bréger, C. P. Grey, and G. Ceder, *Science* 311, 977 (2006).
2. P. G. Bruce, B. Scrosati, and J. M. Tarascon, *Angew. Chem. Int. Ed.* 47, 2930 (2008).

3. J.-P. Zhu, W. Zu, J.-J. Zhao, G. Yang, and Q.-B. Xu, *J. Nanosci. Nanotechnol.* 12, 2539 (**2012**).
4. C. Wang, A. J. Appleby, and F. E. Little, *J. Electroanal. Chem.* 519, 9 (**2002**).
5. P. Verma, P. Maire, and P. Novák, *Electrochim. Acta* 55, 6332 (**2010**).
6. S. Bae, I. Nam, S. Park, Y. G. Yoo, S. Yu, J. M. Lee, J. W. Han, and J. Yi, *ACS Appl. Maters. Interfaces* 7, 16565 (**2015**).
7. N. Ogihara, T. Yasuda, Y. Kishida, T. Ohsuna, K. Miyamoto, and N. Ohba, *Angew. Chem. Int. Ed.* 53, 11467 (**2014**).
8. G. Armstrong, A. R. Armstrong, P. G. Bruce, P. Reale, and B. Scrosati, *Adv. Mater.* 18, 2597 (**2006**).
9. S. H. Kim, H. Park, S. H. Jee, H. S. Ahn, D.-J. Kim, J. W. Choi, S. J. Yoon, and Y. S. Yoon, *Korean J. Chem. Eng.* 26, 485 (**2009**).
10. S. Park, S.-D. Seo, H. J. Kim, C. W. Lee, H. J. Song, S. S. Shin, H. K. Park, K. S. Hong, and D.-W. Kim, *J. Nanosci. Nanotechnol.* 14, 9307 (**2015**).
11. J.-J. Li, Y.-M. Zhang, J.-C. Han, J.-G. Zhou, Z.-H. Zhang, J. Liu, and B. Song, *Mater. Express* 5, 83 (**2015**).
12. G. N. Zhu, H. J. Liu, J. H. Zhuang, C. X. Wang, Y. G. Wang, and Y. Y. Xia, *Energy Environ. Sci.* 4, 4016 (**2011**).
13. S. B. Yoon, H. K. Kim, K. C. Roh, and K. B. Kim, *J. Electrochem. Soc.* 162, A667 (**2015**).
14. L. Ji, Z. Lin, M. Alcoutlabi, and X. Zhang, *Energy Environ. Sci.* 4, 2682 (**2011**).
15. J. Li, S. Xion, Y. Liu, Z. Ju, and Y. Qian, *ACS Appl. Mater. Interfaces* 5, 981 (**2013**).
16. H. Chen, L. Hu, M. Chen, Y. Yan, and L. Wu, *Adv. Funct. Mater.* 24, 934 (**2014**).
17. H. K. Kim, S. M. Bak, and K. B. Kim, *Electrochem. Commun.* 12, 1768 (**2010**).
18. J. Jiang, Y. Feng, N. Mahmood, F. Liu, and Y. Hou, *Sci. Adv. Mater.* 5, 1667 (**2013**).
19. S. Song, P. Huo, W. Fan, W. Shi, and Y. Yan, *Sci. Adv. Mater.* 5, 1801 (**2013**).
20. A. Mondal and N. R. Jana, *Rev. Nanosci. Nanotechnol.* 3, 177 (**2014**).
21. D. C. Marcano, D. V. Kosynkin, J. M. Berlin, A. Sinitskii, Z. Sun, A. Slesarev, L. B. Alemany, W. Lu, and J. M. Tour, *ACS Nano* 4, 4806 (**2010**).
22. G. Kresse and J. Furthmüller, *Phys. Rev. B* 54, 11169 (**1996**).
23. J. P. Perdew, K. Burke, and M. Ernzerhof, *Phys. Rev. Lett.* 77, 3865 (**1996**).
24. P. E. Blöchl, *Phys. Rev. B* 50, 17953 (**1994**).
25. S. Grimme, *J. Comput. Chem.* 27, 1787 (**2006**).
26. L. Wang, T. Maxisch, and G. Ceder, *Phys Rev. B* 73, 195107 (**2006**).
27. U. Aschauer, J. Chen, and A. Selloni, *Phys. Chem. Chem. Phys.* 12, 12956 (**2010**).
28. J. Qiu, P. Zhang, M. Ling, S. Li, P. Liu, H. Zhao, and S. Zhang, *ACS Appl. Mater. Interfaces* 4, 3636 (**2012**).
29. M. Fang, K. Wang, H. Lu, Y. Yang, and S. Nutt, *J. Mater. Chem.* 19, 7098 (**2009**).
30. Y. Qian, A. Vu, W. Smyrl, and A. Stein, *J. Electrochem. Soc.* 159, A1135 (**2012**).